Novel Three-Port Converter With High-Voltage Gain

Li-Jhan Chien, Chien-Chih Chen, Jiann-Fuh Chen, *Senior Member, IEEE*, and Yi-Ping Hsieh

***Abstract*—In this paper, a novel three-port converter (TPC) with high-voltage gain for stand-alone renewable power system applications is proposed. This converter uses only three switches to achieve the power flow control. Two input sources share only one inductor. Thus, the volume can be reduced. Besides, the conversion ratio of the converter is higher than other TPCs. Thus, the degree of freedom of duty cycle is large. The converter can have a higher voltage gain for both low-voltage ports with a lower turns ratio and a reasonable duty ratio. The voltage stress of switches is low; thus, conduction loss can be further improved by adopting low $R_{ds(on)}$ switches. Therefore, the converter can achieve a high conversion ratio and high efficiency at the same time. The operation principles, steady-state analysis, and control method of the converter are presented and discussed. A prototype of the proposed converter with a low input voltage 24 V for photovoltaic source, a battery port voltage 48 V, and an output voltage 400 V is implemented to verify the theoretical analysis. The power flow control of the converter is also built and tested with a digital signal processor.**

***Index Terms*—Bidirectional, high-voltage gain, three-port converter (TPC).**

I. Introduction

DUE to the worldwide development and increment of population, energy resources have become more and more important. Using traditional energy sources, like fossil fuels, may cause air pollution and global warming. Since the amount of the fossil fuel is limited, renewable power systems have been rapidly developed recently [1], [2]. Photovoltaic (PV) system is one of the popular renewable energy sources [3], [4]. Because of the intermittent nature, the PV source cannot provide sufficient power when the load varies rapidly. Therefore, energy storage elements, such as batteries, are used to smoothly supply energy to load in stand-alone renewable power system applications [5]–[7].

Fig. 1(a) shows a conventional stand-alone PV system with a low dc input voltage source and a storage element [8], [9]. The PV source and battery are low-voltage sources, thus the converters have to boost the voltages to match the load [10]. The system needs two converters at the front end. One is an unidirectional converter used to track maximum power point (MPP) and boost the input voltage. The other is a bidirectional converter used to control the power flow between the dc bus and the battery. This system with two conversion stages leads to more components, and larger volume. Fig. 1(b) shows a stand-alone PV system with a TPC and a battery backup. Many topologies have been proposed for renewable energy power systems with the battery backup or hybrid energy source and storage systems [11]–[28].

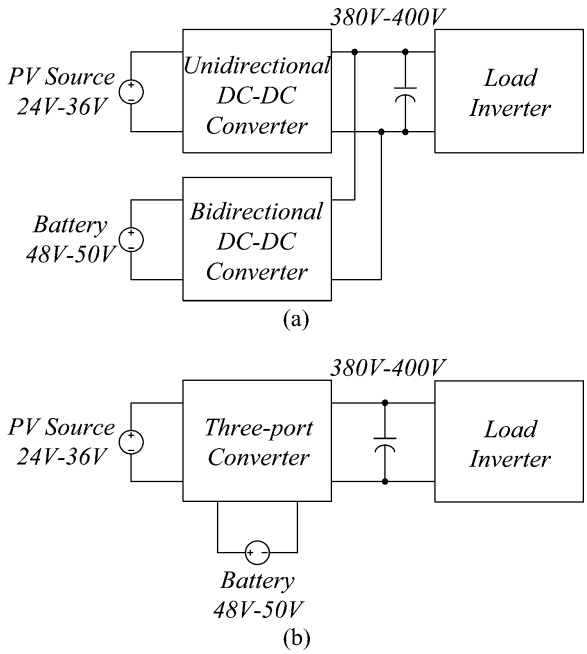

Fig. 1. Stand-alone renewable power systems: (a) with two separated converters and (b) with a TPC.

The isolated topologies are derived by transformers, and there are two kinds of isolated TPCs. Fully isolated TPCs can accommodate different port voltage levels, and provide electrical isolation for each port [11]–[16]. By using phase shift control method, the converter can achieve zero voltage switching (ZVS) on all switches [11]–[15]. A resonant TPC can also be adopted to achieve higher efficiency [16]. However, the converters use a lot of power devices because of the adoption of the full-bridge architecture. And the control methods for the fully isolated TPCs are complex. Therefore, three-port half-bridge converters (TPHBC) with partially electrical isolation is proposed to reduce component count and simplify the control method [17]–[21]. A duty-cycle shift control method is proposed to simplify the control of the TPHBCs [17]. The duty-cycle shift control with phase shift control method can also adopted to achieve ZVS [21]. However, the battery port of the converter is always in use during all operation modes. Therefore, it reduces the life time of battery. Furthermore, the voltage gain of the isolated TPCs is heavily dependent on turns ratio, and high power dissipation may be

Manuscript received July 31, 2013; revised September 11, 2013; accepted September 30, 2013. Date of current version April 30, 2014. This work was supported by the National Science Council, Taiwan, under Award NSC 102-2622-E-006-006-CC2. Recommended for publication by Associate Editor D. Vinnikov.

The authors are with the Green Energy Electronics Research Center, Department of Electrical Engineering, National Cheng Kung University, Tainan, Taiwan (e-mail: lennon0855@gmail.com; et781114@hotmail.com; chenjf@mail.ncku.edu.tw; kyo124718@yahoo.com.tw).

Color versions of one or more of the figures in this paper are available online at http://ieeexplore.ieee.org.

Digital Object Identifier 10.1109/TPEL.2013.2285477

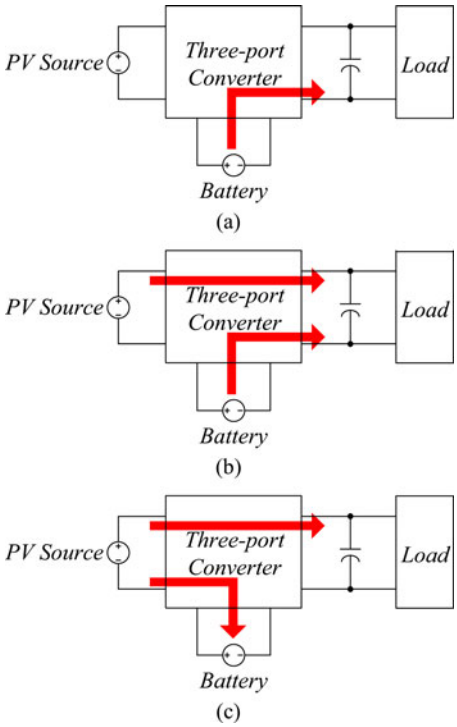

Fig. 2. Operation modes for TPCs: (a) SISO mode, (b) DISO mode, and (c) SIDO mode.

caused by the leakage inductor of the transformer. On the other hand, some of the nonisolated topologies are modified from combining two converters [22]–[24], but the component count is still high. Some nonisolated multiport converters are proposed to combine two converters and reduce components [25]–[27], but the converters do not offer a bidirectional port for battery usage. Thus, it is not suitable for stand-alone renewable power system applications. To reduce the component count, TPCs with single inductor technique are proposed [28]–[30], but the degree of modulation of duty cycle is limited. Thus, the voltage gain is limited [31]–[33].

In this paper, a novel nonisolated TPC with high-voltage gain is proposed. By adjusting the turns ratio of coupled inductor, the converter can provide a higher conversion ratio for both low input voltage ports under a reasonable duty ratio. Furthermore, because it has only one inductor, the power flow between the PV source and battery can be controlled by a simple control method.

In Sections II and III, the operating principle and steady-state analysis of the proposed converter are presented. The control methods are proposed in Section IV. The experimental results are presented in Section V.

II. The Operation of Proposed TPC

A. Power Flow of the TPCs

As shown in Fig. 2, there are three different operation modes for standard TPCs:

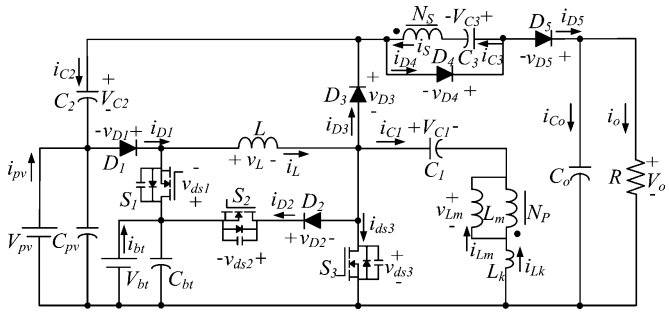

Fig. 3. Proposed Converter Topology.

1) Single input single output (SISO) mode: The battery provides energy to the load alone if there is no radiation received by the PV panel.
2) Double input single output (DISO) mode: PV source and battery provide energy to the load together.
3) Single input double output (SIDO) mode: PV source provides energy to the load, and the battery stores unconsumed power from PV source.

B. Proposed TPC

The proposed converter is shown in Fig. 3. This circuit has three power switches, five diodes, one coupled inductor, one inductor, and three capacitors. V_{pv} is primary input source, and V_{bt} is secondary input source connected to a bidirectional port. The coupled inductor is modeled as a magnetizing inductor L_m, leakage inductance L_k, and an ideal transformer N_p/N_s. The capacitor C_1 can balance the magnetic energy of magnetizing inductor L_m. The diode D_1 and capacitor C_2 form a lossless snubber with leakage inductance energy recycle. The capacitor C_3 and the secondary-side of coupled-inductor N_s form a step-up cell to provide extra voltage gain. The voltages V_{pv}, V_{C2}, v_{Ns}, and V_{C3} are connected in series to build up a high output voltage.

In order to simplify the circuit analysis, the converter is analyzed in continuous-conduction mode (CCM), and the following conditions are assumed:

1) voltage V_{bt} is higher than V_{pv}. (A 250-W PV panel has a MPP voltage about 30 V, and the voltage of a set of lead-acid battery is usually higher than 48 V);
2) capacitors C_1, C_2, C_3, and C_o are large enough that V_{C1}, V_{C2}, V_{C3}, and V_{Co} can be considered as constant voltages (CV);
3) the power MOSFETs and diodes are ideal, but the drain-to-source parasitic capacitor of the MOSFET C_{ds} is considered;
4) the turns ratio of the coupled-inductor n is equal to N_s/N_p;
5) the coupling coefficient of the coupled-inductor k is equal to $L_m/(L_m + L_k)$.

C. Operating Principle of SISO Mode

Figs. 4 and 5 show typical waveforms and current-flow paths of operating modes of SISO mode. Switch S_3 is the main switch.

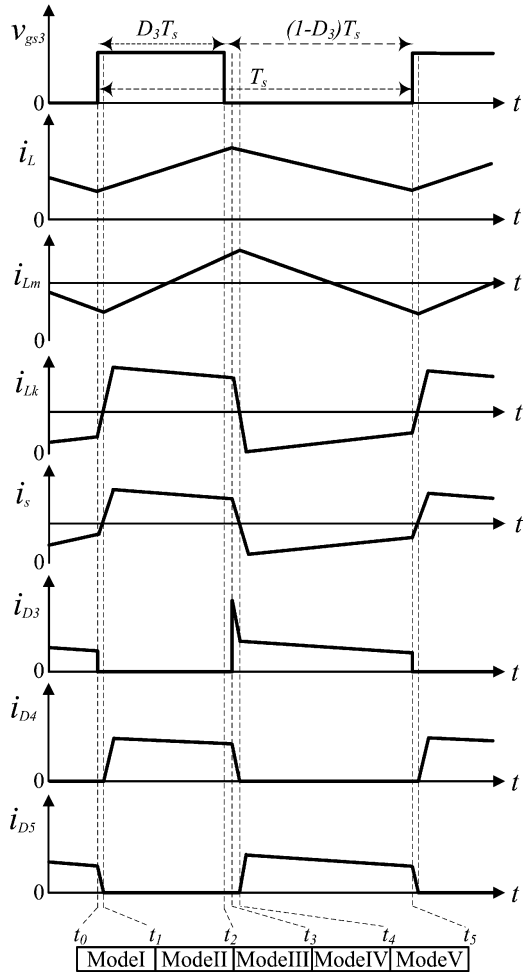

Fig. 4. Typical waveforms in SISO mode at CCM.

Switch S_2, and diodes D_1 and D_2 are always turned OFF in this mode. The operating modes are described as follows:

1) *Mode I [t_0, t_1]:* S_3 is turned ON. Due to the leakage inductance L_k, the secondary-side current of the coupled-inductor i_s decreases linearly. Therefore, diode D_5 is still turned ON and diodes D_3 and D_4 are turned OFF. The current-flow path is shown in Fig. 5(a). L is charged by V_{bt}. Voltages V_{pv}, V_{C2}, v_{Ns}, and V_{C3} are connected in series to charge output capacitor C_o and provide energy to the load R. When i_s is equal to zero at $t = t_1$, this mode ends.
2) *Mode II [t_1, t_2]:* S_3 is turned ON. D_3 and D_5 are turned OFF, and D_4 is turned ON. The current-flow path of this mode is shown in Fig. 5(b). L is charged by V_{bt}. When the magnetic inductor current i_{Lm} decreases to zero, its direction changes. C_1 charges L_m and L_k through S_3. C_3 is charged by C_1 through the secondary-side winding N_s and $D_4, V_{C3} = nV_{C1}$. This mode ends when S_3 is turned OFF at $t = t_2$.
3) *Mode III [t_2, t_3]:* S_3 is turned OFF, the parasitic capacitor of S_3, C_{ds3}, is charged by both inductor current i_L and leakage inductance current i_{Lk}. The current-flow path of this stage is shown in Fig. 5(c). C_3 is still charged by

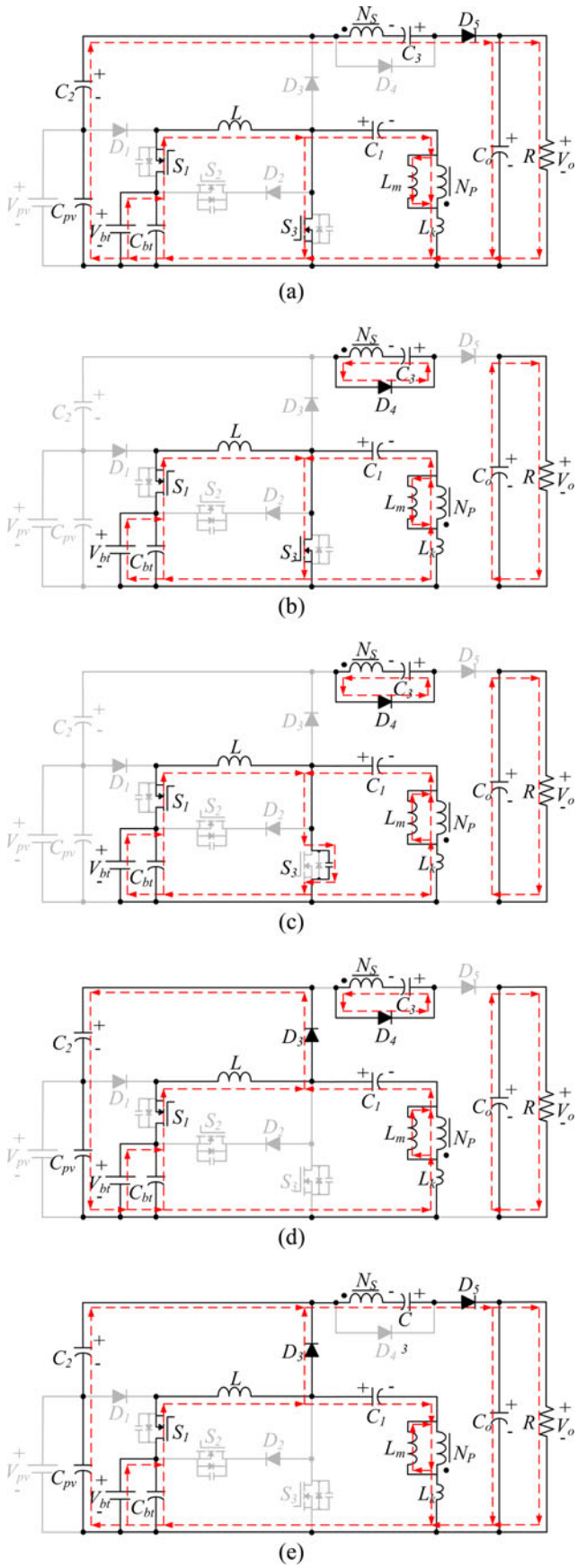

Fig. 5. Current-flow paths of operating modes in SISO mode: (a) mode I, (b) mode II, (c) mode III, (d) mode IV, and (e) mode V.

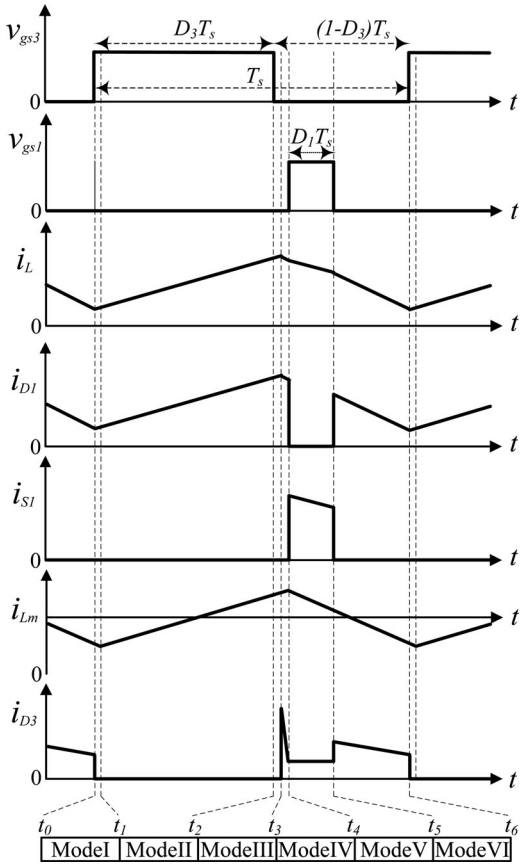

Fig. 6. Typical waveforms in DISO mode at CCM.

C_1 through N_s and D_4. This mode ends when $v_{ds3} = V_{in} + v_L$ at $t = t_3$.

4) *Mode IV [t_3, t_4]:* S_3 is still turned OFF. D_3 is turned ON to recycle energy from L_k to C_2. The current-flow path is shown in Fig. 5(d). The secondary-side current i_s still charges C_3; therefore, D_5 remains open. When $i_s = 0$ at $t = t_4$, D_4 is cut off, and this mode ends.
5) *Mode V [t_4, t_5]:* S_3 is still turned OFF. D_5 is turned ON. The current-flow path of this mode is shown in Fig. 5(e). C_1 is charged by V_{bt} and L. The secondary-side of the coupled-inductor induces a high voltage v_{Ns}, which is connected in series with capacitors V_{pv}, C_2, and C_3 to build up a high output voltage. C_2 is recharged by L through D_3. This mode ends when S_3 is turned ON at $t = t_5$.

D. Operating Principle of DISO Mode

Figs. 6 and 7 show typical waveforms and current-flow paths of the operating modes of DISO mode. Most of the modes are similar to those in SISO mode, the major difference is a two-stage discharging of inductor L when S_3 is turned OFF. S_2 and D_2 are always turned OFF. S_3 is a MPPT switch and S_1 is used to regulate the output voltage. The operating modes are described as follows:

1) *Mode I [t_0, t_1]:* S_3, D_1, and D_5 are turned ON; S_1, D_3, and D_4 are turned OFF. The current-flow path is shown in

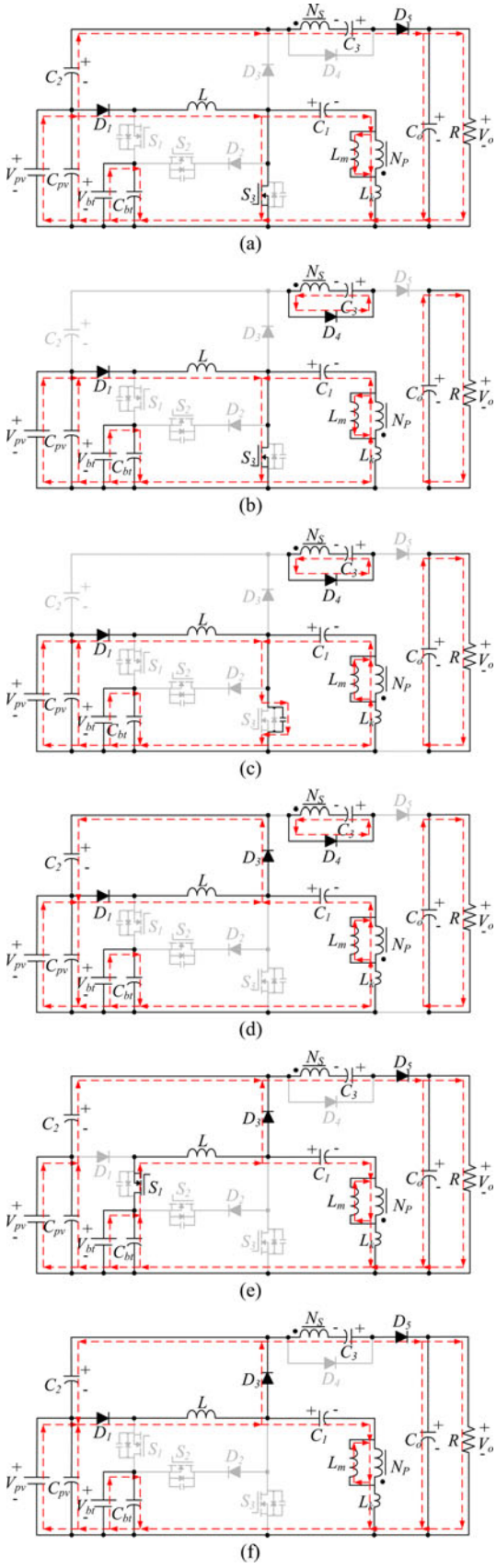

Fig. 7. Current-flow paths of operating modes in DISO mode: (a) mode I, (b) mode II, (c) mode III, (d) mode IV, (e) mode V, and (f) mode VI.

Fig. 7(a). Thus, inductor L is charged by V_{pv}. When $i_s = 0$ at $t = t_1$, this mode ends.

2) *Mode II [t_1, t_2]:* S_3, D_1, and D_4 are turned ON. S_1, D_3 and D_5 are turned OFF. The current-flow path of this mode is shown in Fig. 7(b). L is charged by V_{pv}. C_1 charges L_m and L_k through S_3. C_3 is charged by C_1 through N_s, and $V_{C3} = nV_{C1}$. This mode ends when S_3 is turned OFF at $t = t_2$.
3) *Mode III [t_2, t_3]:* After S_3 is turned OFF, C_{ds3} is charged by i_L and i_{Lk}. The current-flow path of this stage is shown in Fig. 7(c). C_3 is still charged by C_1 through N_s and D_4. This mode ends when $v_{ds3} = V_{in} + v_L$ at $t = t_3$.
4) *Mode IV [t_3, t_4]:* S_3 is turned OFF. D_3 is turned ON to recycle energy from L_k to C_2. The current-flow path is shown in Fig. 7(d). The secondary-side current i_s still charges C_3. When S_1 is turned ON, this mode ends at $t = t_4$.
5) *Mode V [t_4, t_5]:* S_3 and D_1 are turned OFF. S_1 and D_5 are turned ON. The current-flow path of this mode is shown in Fig. 7(e). The voltage variation of the input source causes a variation of different negative slope of the inductor current i_L. Battery port releases energy to the load through L. C_1 is also charged by V_{bt} and L. Voltages V_{pv}, V_{C2}, v_{Ns}, and V_{C3} are connected in series to charge C_o and provide energy to the load. This mode ends when S_1 is turned OFF at $t = t_5$.
6) *Mode VI [t_5, t_6]:* S_1 and S_3 are turned OFF. D_1, D_3, and D_5 are turned ON. The current-flow path of this mode is shown in Fig. 7(f). The negative slope of i_L is changed again because of input voltage variation. C_1 is charged by V_{pv} and L. C_2 is recharged by L through D_1 and D_3. This mode ends when S_3 is turned ON at $t = t_6$.

E. Operating Principle of SIDO Mode

Figs. 8 and 9 show typical waveforms and current-flow paths of operating modes of SIDO mode. Most of the modes are similar to those in DISO mode, the only difference is a two-stage discharging of inductor L. S_1 is always turned OFF. S_3 is MPPT switch and S_2 is used to regulate the output voltage. The operating modes are described as follows:

1) *Mode I [t_0, t_1] and Mode II [t_1, t_2]:* The current-flow paths of these stages are shown in Fig. 9(a) and (b). These two modes are identical to the Mode I and Mode II in DISO mode.
2) *Mode III [t_2, t_3]:* S_3 is turned OFF and C_{ds3} is charged by i_L and i_{Lk}. S_2 is turned ON, but D_2 is turned OFF. The current-flow path of this stage is shown in Fig. 9(c). C_3 is still charged by C_1 through N_s. This mode ends when $v_{ds3} = V_{bt}$ at $t = t_3$.
3) *Mode IV [t_3, t_4]:* S_3 is turned OFF. S_2 and D_2 are turned ON. V_{PV} and L release energy to the battery port. The current-flow path of this stage is shown in Fig. 9(d). The voltage across the primary-side of the coupled-inductor is equal to $V_{bt} - V_{C1}$, and $v_{ds3} = V_{bt}$. Therefore, diodes D_3, D_4, and D_5 are all turned OFF. On the other hand, since there is no current flowing into the ideal transformer $N_p/N_s, L_m$ is considered as a normal inductor and releases its energy to the battery port. This mode ends when S_2 is turned OFF at $t = t_4$.
4) *Mode V [t_4, t_5]:* S_2 and S_3 are turned OFF. Currents i_L and i_{Lm} charge C_{ds2} and C_{ds3}. The current-flow path of this stage is shown in Fig. 9(e). There is no current flowing into N_p/N_p, and diodes D_4 and D_5 are turned OFF. When $v_{ds3} = V_{pv} + V_{C2}$ at $t = t_5$, this mode ends.
5) *Mode VI [t_5, t_6] & Mode VII [t_6, t_7]:* The current-flow paths of these stages are shown in Fig. 9(f) and (g). These two modes are identical to the Mode IV and Mode VI in DISO mode.

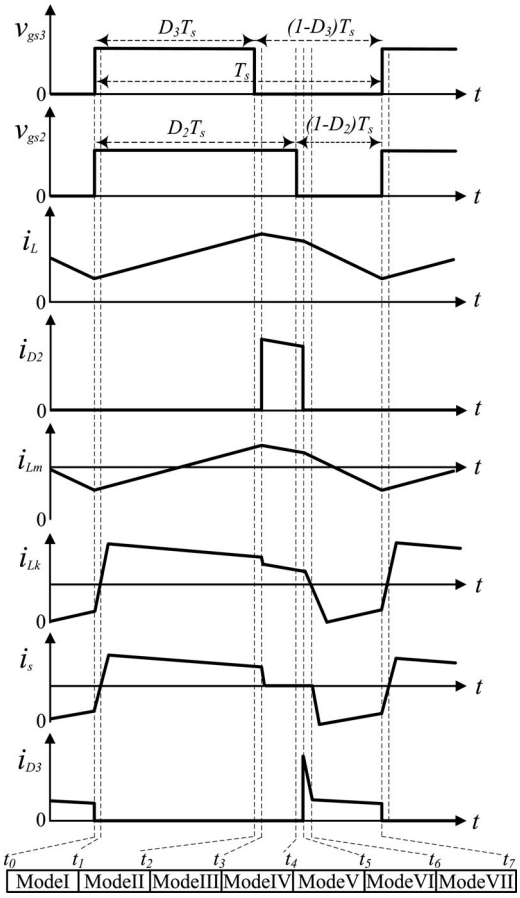

Fig. 8. Typical waveforms in SIDO mode at CCM.

III. Steady-State Analysis of the Proposed Converter

To simplify the analysis, the leakage inductance L_k is ignored, and the analysis only considers switch in ON and OFF condition. The symbols D_{s1}, D_{s2}, and D_{s3} showed in this section represent the duty ratios of switches S_1, S_2, and S_3, respectively.

A. SISO Mode

When S_3 ON

$$V_L = V_{bt} \tag{1}$$

$$V_{Lm} = V_{C1} \tag{2}$$

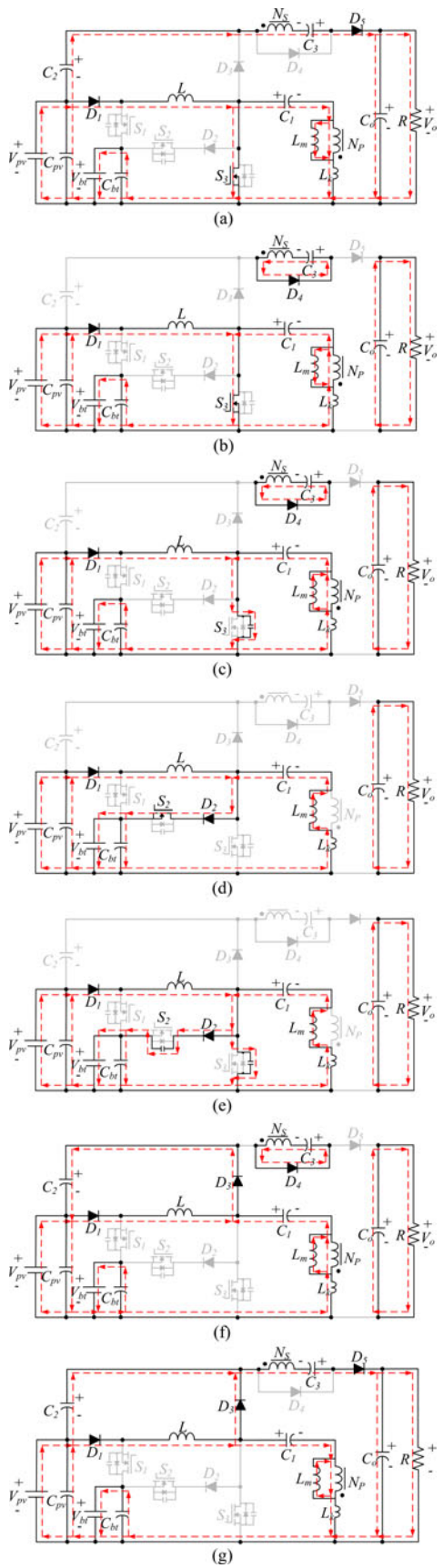

Fig. 9. Current-flow paths of operating modes in SIDO mode: (a) mode I, (b) mode II, (c) mode III, (d) mode IV, (e) mode V, (f) mode VI, and (g) mode VII.

$$V_{C3} = V_{Ns} = nV_{Lm} = nV_{C1}. \tag{3}$$

When S_3 OFF

$$V_L = V_{bt} - V_{ds3} = V_{bt} - (V_{C2} + V_{pv}) \tag{4}$$

$$V_{Lm} = V_{C1} - V_{ds3} = V_{C1} - (V_{C2} + V_{pv}) \tag{5}$$

$$nV_{Lm} = n\left[V_{C1} - (V_{C2} + V_{pv})\right] \tag{6}$$

$$D_{s3}V_{bt} = V_L(1 - D_{s3}) \Rightarrow V_L = \frac{D_{s3}V_{bt}}{1 - D_{s3}} = (V_{C2} + V_{pv}) - V_{bt} \tag{7}$$

$$D_{s3}V_{C1} = V_{Lm}\,(1 - D_{s3}) \Rightarrow V_{Lm} = \frac{D_{s3}V_{C1}}{1 - D_{s3}}. \tag{8}$$

By applying voltage balance principle on inductor L and magnetic inductor L_m, the following equations can be obtained

$$D_{s3}V_{bt} + (1 - D_{s3})\,(V_{bt} - V_{ds3}) = 0 \tag{9}$$

$$D_{s3}V_{C1} + (1 - D_{s3})\,(V_{C1} - V_{ds3}) = 0 \tag{10}$$

$$V_{C1} = V_{bt}. \tag{11}$$

Therefore,

$$V_o = V_{pv} + V_{C2} + V_{Ns} + V_{C3} \tag{12}$$

$$V_o = \frac{1 + n}{1 - D_{s3}}. \tag{13}$$

By applying the same technique to other two modes, the voltage gain of DISO mode and SIDO mode can also be obtained.

B. DISO Mode

$$D_{s3}V_{pv} + D_{s1}(V_{bt} - V_{C2} - V_{pv})(1 - D_{s3} - D_1) \times (-V_{C2}) = 0 \tag{14}$$

$$D_{s3}V_{C1} + (1 - D_{s3})(V_{C1} - V_{C2} - V_{pv}) = 0 \tag{15}$$

$$V_{C1} = V_{pv} + D_{s1}(V_{bt} - V_{pv}). \tag{16}$$

Therefore,

$$V_o = \frac{(1 + n)}{1 - D_{s3}}\left[(1 - D_{s1})V_{pv} + D_{s1}V_{bt}\right]. \tag{17}$$

C. SIDO Mode

$$D_{s3}V_{pv} + (D_{s2} - D_{s3})\,(V_{pv} - V_{bt}) + (1 - D_{s2}) \times (-V_{C2}) = 0 \tag{18}$$

$$D_{s3}V_{C1} + (D_{s2} - D_{s3})(V_{C1} - V_{bt}) + (1 - D_{s2})(V_{C1} - V_{C2} - V_{pv}) = 0 \tag{19}$$

$$V_{C1} = V_{pv}. \tag{20}$$

Therefore

$$V_o = \frac{1 + n}{1 - D_{s2}}\left[V_{pv} - V_{bt}(D_{s2} - D_{s3})\right] \tag{21}$$

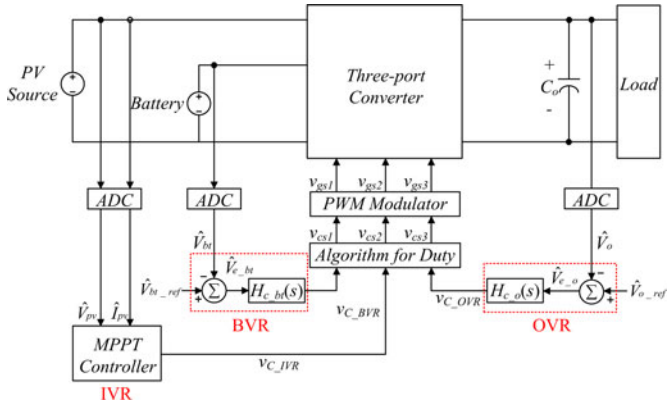

Fig. 10. Control diagram for the proposed converter.

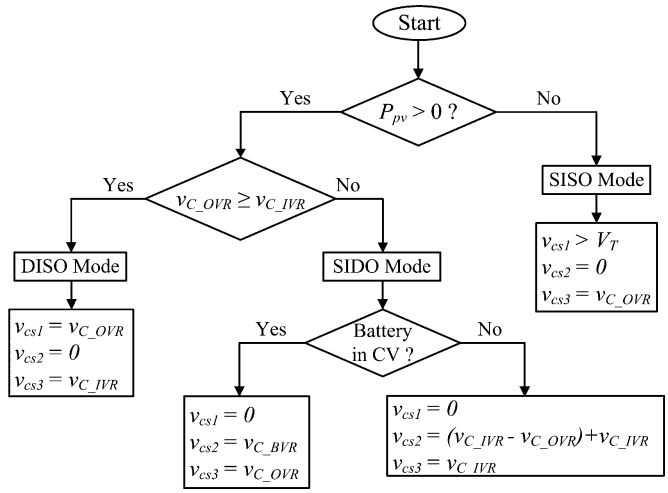

Fig. 11. Algorithm flow chart for the proposed converter.

compares the conversion ratio of [28] with the proposed converter, it is clear that the proposed converter can provide a higher voltage gain under the same duty ratio. The voltage stress on the switch S_3 also can be obtained easily

$$V_{ds3} = \frac{(1 - D_{s1})\, V_{pv} + D_{s1} V_{bt}}{1 - D_{s3}} \qquad \text{[DISO mode]} \quad (22)$$

$$V_{ds3} = \frac{V_{pv} - V_{bt}\,(D_{s2} - D_{s3})}{1 - D_{s2}} \qquad \text{[SIDO mode].} \quad (23)$$

IV. Construction of Digital Control

A control diagram for the proposed converter is showed in Fig. 10. There are three regulators in the proposed control method: input PV voltage regulator (IVR) for MPPT, battery voltage regulator (BVR) for battery voltage limitation, and output voltage regulator (OVR) for output voltage control. The battery port is assumed to be able to sink all the current from PV port at MPP. The IVR is a MPPT algorithm with perturb and observe (P&O) technique. The BVR and OVR are two voltage mode control loops used to regulate voltages of battery port and output port, respectively.

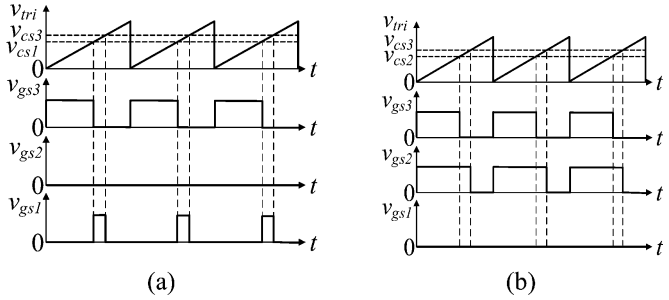

Fig. 12. PWM modulator for the proposed converter: (a) DISO mode and (b) SIDO mode.

Fig. 11 shows an algorithm for calculating the duty ratios for the switches. If there is no energy provided by the PV source, then the converter is operated in SISO mode. In the SISO mode, switch S_3 is used to regulate the output voltage; therefore, $v_{cs3} = v_{C\_OVR}$. If the PV source starts to provide energy, switch S_3 is used to regulate the input voltage V_{pv} and track MPP. Thus, $v_{cs3} = v_{C\_IVR}$ in both the DISO and SIDO modes. However, if the battery port is in CV charging mode, then switch S_3 is used to regulate the output voltage.

Since v_{C_IVR} is used to track the MPP, the determination of operation mode depends on v_{C_OVR}. Comparing signals v_{C_OVR} and v_{C_IVR}, if feedback voltage of output voltage is lower than the reference, then $v_{C\_OVR} \geq v_{C\_IVR}$. It means that the demand for output power P_o is higher than the input power provided by the PV port. Thus, the converter is operated in DISO mode. And the control signal of switch S_1, v_{cs1}, is equal to v_{C_OVR}. Thus, the duty ratio of switch S_1 increases as the P_o increases, and the battery port provides extra energy to the output. The generation of the control signals in DISO mode is showed in Fig. 12(a). If $P_o = P_{pv}$, then $v_{C\_OVR} = v_{C\_IVR}$. Switches S_1 and S_2 are turned OFF, and the converter is operated like a traditional two-port converter.

On the other hand, if $v_{C\_OVR} \leq v_{C\_IVR}$, it means that output voltage is too high because the extra energy charges output capacitor C_o, and the converter is operated in SIDO mode. The control signal of switch S_2, v_{cs2}, can be determined by the following equation: $v_{cs2} = (v_{C\_IVR} - v_{C\_OVR}) + v_{C\_IVR}$. Thus, the duty ratio of switch S_2 increases as the P_o decreases, and the battery port sinks extra energy from the PV port. The generation of the control signals in SIDO mode is showed in Fig. 12(b). Therefore, the converter can have a smooth transition without causing an overshoot on output voltage.

If the battery is in CV charging in SIDO mode, then both switches are used to regulate the voltages because the battery port cannot sink the extra power from the PV source. The controller $H_{c\_bt(s)}$ only operates when the battery voltage reaches its maximum value, and the battery is in a CV charging condition. The compensator of the voltage mode controller $H_{c\_bt(s)}$ is designed under a very light load condition to simulate CV charging state. Once the converter operates in CV charging mode in DISO mode, the control signals are generated by controllers, $H_{c\_o(s)}$ and $H_{c\_bt(s)}$, where $v_{cs2} = v_{C_BVR}$ and $v_{cs3} = v_{C\_OVR}$.

TABLE I
CIRCUIT SPECIFICATION

Voltage of PV port V_{pv}	24 V
Voltage of battery port V_{bt}	48 V
Voltage of load V_o	400 V
Maximum output power $P_{o,max}$	300 W
Boundary output current I_{OB}	0.3 A
Switching frequency f_s	50 kHz
Controller: DSP	TMS320F28035

TABLE II
SPECIFICATION FOR DELSOLAR/D6M250 B3 A

Maximum Power : P_{max}	250 W
Rated Voltage : V_{MPP}	30.60 V
Rated Current : I_{MPP}	8.17 A
Open Circuit Voltage : V_{OC}	37. 85 V
Short Circuit Current : I_{SC}	8.58 A

V. EXPERIMENTAL RESULTS

To verify the performance of the proposed converter, a prototype circuit is implemented and tested in the laboratory. The specification for the converter is shown in Table I. And the specification for PV panel for the testing is shown in Table II.

A. Waveforms Measured in SISO Mode

The key waveforms of proposed converter at full-load $P_o = 300$ W are shown in Fig. 13.

Fig. 13(a) shows that when S_3 is turned ON, D_4 is turned ON to charge C_3. When S_3 is turned OFF, D_4 is turned OFF and D_5 is turned ON to charge the output capacitor. Fig. 13(b) shows that at the beginning of the switch-off period, D_3 is turned ON to recycle the energy from L_k with a spike current. Fig. 13(c) shows that when S_3 is turned ON, L and L_k store energy, i_s charges C_3. When S_3 turned OFF, L releases energy. The voltage spike across S_3 is less than 90 V. Therefore, a low $R_{DS(ON)}$ switch can be adopted to reduce conduction loss.

B. Waveforms Measured in DISO Mode

The key waveforms of proposed converter in DISO are shown in Fig. 14. The power P_{pv} of the PV source is kept at MPP, and $P_o > P_{pv}$.

Fig. 14(a) shows voltage and current waveforms of diodes D_3 and D_4. After switch S_1 is turned OFF, i_{D3} increases abruptly. Fig. 14(b) shows that there is a two-stage discharging for i_L when S_3 is turned OFF, and currents i_{D1} and i_{S1} correspond to the currents from the PV and battery port, respectively.

C. Waveforms Measured in SIDO Mode

The key waveforms of the proposed converter in SIDO are shown in Fig. 15. P_{pv} is kept at MPP, and $P_{pv} > P_o$.

Fig. 15(a) shows voltage and current waveforms of diodes D_3 and D_4. After S_2 is turned OFF, diode D_3 is turned ON to start the second-stage discharge of inductor L. Fig. 15(b) shows that during the off-period of S_3, currents i_L and i_{Lm} flow into the battery port first. After S_2 is turned OFF, output diode D_5 is turned ON to provide energy to the load.

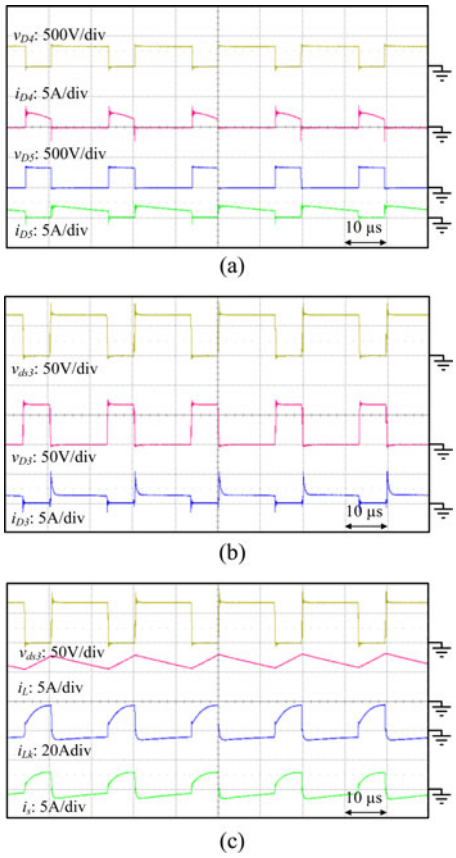

Fig. 13. Waveforms in SISO mode under full-load $P_o = 300$ W: (a) waveforms of diodes D_4 and D_5, (b) waveforms of diode D_3, and (c) waveforms of main currents.

D. MPP Tracking

To verify that the converter is able to track the MPP and regulate the output voltage with two different input sources simultaneously, a solar array simulator is connected to the PV port and a dc power supply is connected to the battery port. Fig. 16 shows the tracking curve in SIDO mode, where the solar irradiation is set to 1000 W/m^2. The tracking points are recorded by the simulator at MPP, the recording time is 60 s. The voltage and current of the PV port V_{pv}, i_{pv}, and the voltage of battery port V_{bt} are shown in Fig. 17. During the start-up of battery port, a disturbance interferes in the MPP tracker. However, the converter still can track the MPP after a short period of time. Moreover, the proposed converter is a current-fed converter with continuous-conduction current on the low voltage side. This helps the converter to track the MPP more easily in SIDO mode, but it does not help in DISO mode since the input current from the PV port is not continuous. Therefore, the ripples of voltage and current waveforms shown in Fig. 17 is enlarged once the converter operates under the double input situation.

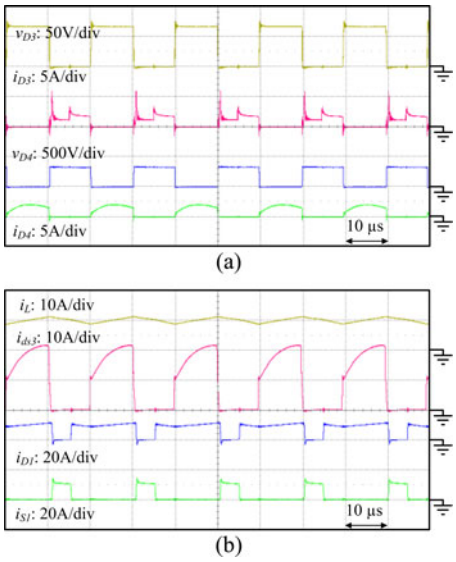

Fig. 14. Waveforms in DISO mode: (a) waveforms of diodes D_3 and D_4 and (b) waveforms of key currents.

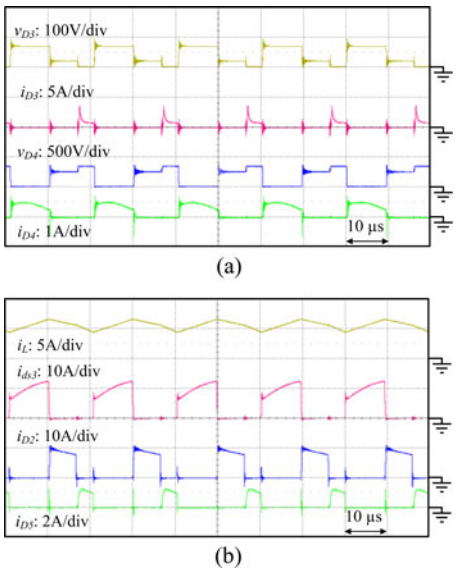

Fig. 15. Waveforms in SIDO mode: (a) waveforms of diodes D_3 and D_4 and (b) waveforms of key currents.

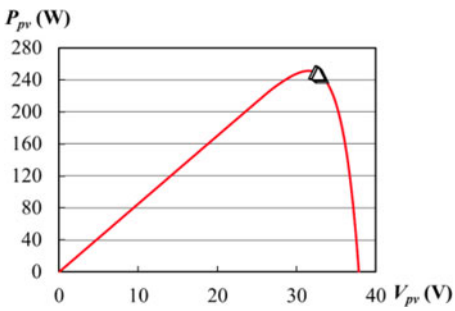

Fig. 16. P–V tracking curve in the DISO mode.

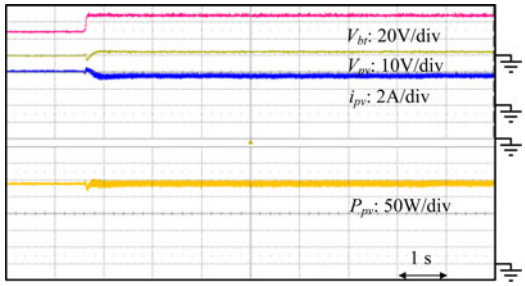

Fig. 17. Waveforms of start-up of battery in DISO mode.

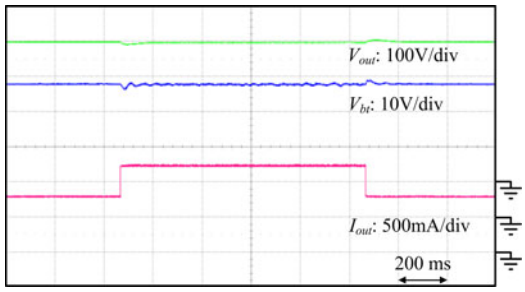

Fig. 18. Load variation between $P_o = 120$ W and $P_o = 300$ W in SIDO mode.

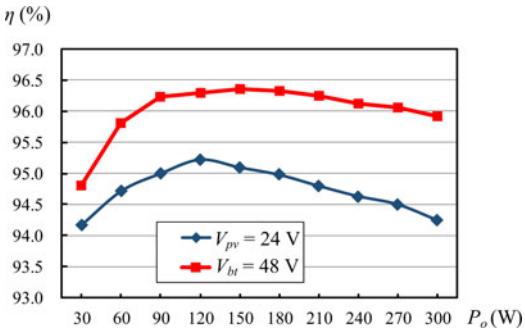

Fig. 19. Conversion efficiency in SISO mode.

E. Experimental Results in SIDO Mode With CV Charging

Fig. 18 shows the load variation between 40% load $P_o = 120$ W and full-load $P_o = 300$ W. In order to simulate the condition of CV charging to the battery port, the battery port operates at a very light load $i_{bt} = 0.05$ A. The voltage variation of the battery port is less than 2 V.

F. Conversion Efficiency

Fig. 19 shows the conversion efficiency of the converter in SISO mode from both input ports. The conversion efficiency η increases when input voltage increases. The highest efficiency is 96.35% at $P_o = 150$ W with $V_{in} = 48$ V. The overall efficiency is above 94% for both input port and different input voltages. Fig. 20 shows the system conversion efficiency in DISO and SIDO mode. P_{pv} is kept at MPP while the output power P_o varies from 53.33 to 320 W. The converter is operated in DISO mode only when $P_o = 266.67$ W and $P_o = 320$ W, and the rest of the efficiency is measured in SIDO mode. The highest efficiency

Fig. 20. Conversion efficiency under constant P_{pv} and various P_o.

is 93.92% at $P_o = 228.57$ W, where most of the energy from the PV port is delivered to the load R, and the converter operated like a two-port converter. The overall efficiency is above 93%.

VI. Conclusion

A novel TPC with high-voltage gain is proposed in the paper. The detailed analysis and discussion of the converter are presented. The converter has an input port for a renewable energy source, a bidirectional port for energy storage elements, and an output port for a high-voltage load. The converter can provide a higher conversion ratio for both low input voltage ports with less power switches, a lower turns ratio, a reasonable duty ratio, and a simple control method. The experimental results verify the high step-up function and high efficiency of the converter. The low-voltage inputs of 24 and 48 V can easily be boosted to a high-voltage output of 400 V. The measured waveforms are consistent with the theoretical analysis. The overall efficiency is above 94% measured from both input ports. And the system efficiency at MPP of the PV source is above 93% in both DISO and SIDO mode.

References

[1] D. Vinnikov and I. Roasto, "Quasi-z-source-based isolated dc/dc converters for distributed power generation," *IEEE Trans. Ind. Electron.*, vol. 58, no. 1, pp. 192–201, Jan. 2011.

[2] Y. P. Hsieh, J. F. Chen, T. J. Liang, and L. S. Yang, "Novel high step-up dc–dc converter for distributed generation system," *IEEE Trans. Ind. Electron.*, vol. 60, no. 4, pp. 1473–1482, Apr. 2013.

[3] A. I. Bratcu, I. Munteanu, S. Bacha, D. Picault, and B. Raison, "Cascaded dc–dc converter photovoltaic systems: power optimization issues," *IEEE Trans. Ind. Electron.*, vol. 58, no. 2, pp. 403–411, Feb. 2011.

[4] M. Cacciato, A. Consoli, R. Attanasio, and F. Gennaro, "Soft-switching converter with HF transformer for grid-connected photovoltaic systems," *IEEE Trans. Ind. Electron*, vol. 57, no. 5, pp. 1678–1686, May 2010.

[5] Y. M. Chen, A. Q. Huang, and X. Yu, "A high step-up three-port dc–dc converter for stand-alone PV/battery power systems," *IEEE Trans. Power Electron*, vol. 28, no. 11, pp. 5049–5062, Nov. 2013.

[6] R. J. Wai, R. Y. Duan, and K. H. Jheng, "High-efficiency bidirectional dc–dc converter with high-voltage gain," *IET Power Electron.*, vol. 5, no. 2, pp. 137–184, Feb. 2012.

[7] R. Y. Duan and J. D. Lee, "High-efficiency bidirectional dc–dc converter with coupled inductor," *IET Power Electron*, vol. 5, no. 1, pp. 115–123, Jan. 2012.

[8] K. Sun, L. Zhang, Y. Xing, and J. M. Guerrero, "A distributed control strategy based on dc bus signaling for modular photovoltaic generation system with battery energy storage," *IEEE Trans. Power Electron.*, vol. 26, no. 10, pp. 3032–3045, Oct. 2011.

[9] F. Locment, M. Sechilariu, and I. Houssamo, "DC load and batteries control limitations for photovoltaic systems. experimental validation," *IEEE Trans. Power Electron.*, vol. 27, no. 9, pp. 4030–4038, Sep. 2012.

[10] Y. P. Hsieh, J. F. Chen, T. J. Liang, and L. S. Yang, "A novel high step-up dc–dc converter for a microgrid system," *IEEE Trans. Power Electron.*, vol. 26, no. 4, pp. 1127–1136, Apr. 2011.

[11] D. Liu and H. Li, "A ZVS bidirectional dc–dc converter for multiple energy storage elements," *IEEE Trans. Power Electron.*, vol. 21, no. 5, pp. 1513–1517, Sep. 2006.

[12] Y. M. Chen, Y. C. Liu, and F. Y. Wu, "Multiinput dc/dc converter based on the multiwinding transformer for renewable energy applications," *IEEE Trans. Ind. Appl.*, vol. 38, no. 4, pp. 1096–1104, Jul. 2002.

[13] J. L. Durate, M. Hendrix, and M. G. Simoes, "Three-port bidirectional converter for hybrid fuel cell system," *IEEE Trans. Power Electron.*, vol. 22, no. 2, pp. 480–487, Mar. 2007.

[14] C. Zhao, S. D. Round, and J. W. Kolar, "An isolated three-port bidirectional dc–dc converter with decoupled power flow management," *IEEE Trans. Power Electron.*, vol. 23, no. 5, pp. 2443–2453, Sep. 2008.

[15] H. Tao, A. Kotsopoulos, J. L. Duarte, and M. A. M. Hendrix, "Three-port triple-half-bridge bidirectional converter with zero-voltage switching," *IEEE Trans. Power Electron.*, vol. 23, no. 2, pp. 782–792, Mar. 2008.

[16] K. Haribaran and N. Mohan, "Three-port series-resonant dc–dc converter to interface renewable energy sources with bidirectional load and energy storage ports," *IEEE Trans. Power Electron.*, vol. 24, no. 10, pp. 2289–2297, Oct. 2009.

[17] Z. Qian, O. Abdel-Rahman, H. Al-Atrash, and I. Batarseh, "Modeling and control of three-port DC/DC converter interface for satellite applications," *IEEE Trans. Power Electron.*, vol. 25, no. 3, pp. 637–649, Mar. 2010.

[18] H. Wu, R. Chen, J. Zhang, Y. Xing, H. Hu, and H. Ge, "A family of three-port half-bridge converters for a stand-alone renewable power system," *IEEE Trans. Power Electron.*, vol. 26, no. 9, pp. 2697–2706, Sep. 2011.

[19] A. Hussam, F. Tian, and I. Batarseh, "Tri-modal half-bridge converter topology for three-port interface," *IEEE Trans. Power Electron.*, vol. 22, no. 1, pp. 341–345, Jan. 2007.

[20] Z. Qian, O. Abdel-Rahman, H. Hu, and I. Batarseh, "An integrated four-port dc\dc converter for renewable energy applications," *IEEE Trans. Power Electron.*, vol. 25, no. 7, pp. 1877–1887, Jul. 2010.

[21] F. Z. Peng, H. Li, G. J. Su, and J. S. Lawler, "A new ZVS bidirectional DC–DC converter for fuel cell and battery application," *IEEE Trans. Power Electron.*, vol. 19, no. 1, pp. 54–65, Jan. 2004.

[22] Y. C. Liu and Y. M. Chen, "A systematic approach to synthesizing multiinput dc–dc converters," *IEEE Trans. Power Electron.*, vol. 24, no. 1, pp. 116–127, Jan. 2009.

[23] S. H. Hosseini, S. Danyali, and S. A. K. M. N. F. Nejabatkhah, "Modeling and control of a new three-input dc–dc boost converter for hybrid PV/FC/battery power system," *IEEE Trans. Power Electron.*, vol. 27, no. 5, pp. 2309–2324, May 2012.

[24] R. J. Wai, C. Y. Lin, and Y. R. Chang, "High step-up bidirectional isolated converter with two input power source," *IEEE Trans. Ind. Electron.*, vol. 56, no. 7, pp. 2629–2643, Jul. 2009.

[25] Y. C. Liu and Y. M. Chen, "A systematic approach to synthesizing multiinput dc–dc converters," *IEEE Trans. Power Electron.*, vol. 24, no. 1, pp. 116–127, Jan. 2009.

[26] R. J. Wai, C. Y. Lin, C. Y. Liu, and Y. R. Chang, "High-efficiency single-stage bidirectional converter with multiinput power sources," *IET Power Appl.*, vol. 1, no. 5, pp. 763–777, Sep. 2007.

[27] R. J. Wai, C. Y. Lin, J. J. Liaw, and Y. R. Chang, "Newly designed ZVS multiinput converter," *IEEE Trans. Ind. Electron.*, vol. 58, no. 2, pp. 555–566, Feb. 2011.

[28] H. Wu, K. Sun, S. Ding, and Y. Xing, "Topology derivation of nonisolated three-port dc–dc converter from DIC and DOC," *IEEE Trans. Power Electron.*, vol. 28, no. 7, pp. 3297–3307, Jul. 2013.

[29] Y. M. Chen, Y. C. Liu, and S. H. Lin, "Double-input PWM dc–dc converter for high/low-voltage sources," *IEEE Trans. Ind. Electron.*, vol. 53, no. 5, pp. 1538–1545, Oct. 2006.

[30] H. Wu, K. Sun, R. Chen, H. Hu, and Y. Xing, "Full-bridge three-port converters with wide input voltage range for renewable power systems," *IEEE Trans. Power Electron.*, vol. 27, no. 9, pp. 3965–3974, Sep. 2012.

[31] S. K. Changchien, T. J. Liang, J. F. Chen, and L. S. Yang, "Novel high step-up dc-dc converter for fuel cell energy conversion system," *IEEE Trans. Ind. Electron.*, vol. 57, no. 6, pp. 2007–2017, Jun. 2010.

[32] T. F. Wu, Y. S. Lai, J. C. Hung, and Y. M. Chen, "Boost converter with coupled inductors and buck-boost type of active clamp," *IEEE Trans. Ind. Electron.*, vol. 55, no. 1, pp. 154–162, Jan. 2008.

[33] F. L. Luo, "Six self-lift dc–dc converters, voltage lift technique," *IEEE Trans. Ind. Electron.*, vol. 48, no. 6, pp. 1268–1272, Dec. 2011.

Li-Jhan Chien was born in Taipei, Taiwan, in 1989. He received the B.S. degree and the M.S. degrees in electrical engineering from National Cheng-Kung University, Tainan, Taiwan, in 2011 and 2013, respectively.

He is currently a Design & Development Engineer with the Analog & Imaging IC BU, Semiconductor & Storage Products Company, Toshiba, Japan. His current research fields of interest include bidirectional converters, three-port converters, and renewable energy systems.

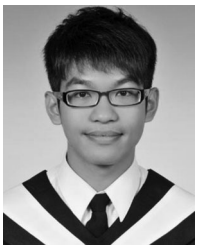

Chien-Chih Chen was born in Taichung, Taiwan, in 1989. He received the B.S. degree in electrical engineering from National Cheng-Kung University (NCKU), Taiwan, in 2012. He is currently working toward the M.S. degree at the NCKU, Taiwan.

His research interests are dc–dc power converter, dc–ac inverter, and renewable energy conversion.

Jiann-Fuh Chen (S'79–M'80–SM'12) was born in ChungHua, Taiwan, in 1955. He received the B.S., M.S., and the Ph.D. degrees in electrical engineering from National Cheng-Kung University (NCKU), Tainan, Taiwan, in 1978, 1980, and 1985, respectively.

He is currently a Professor of electrical engineering and directs the Academia–Industry Consortium Center and Incubator Center at Tainan Science Park, Taiwan. He is also a Chairman of Taiwan Power Electronics Association, and a Governor of Kaohsiung section of the Chinese Institute of Electrical Engineering. Since 2010, he acts as Convener of Electrical Power Program of National Science Council (NSC), Taiwan. He has served at NCKU in various capacities that include Director of Electrical Laboratories from 1996 to 1999, Manager of the Business section of Research and Services Headquarter from 1998 to 2000, Supervisor of the Engineering Division section of National Cheng-Kung Hospital from 2000 to 2001, the Director of Business Incubator Center from 2003 to 2006, and the Chairman of Electrical Engineering Department from 2008 to 2011. He leads over 20 research projects sponsored by NSC Taiwan. He has published one book, more than 50 journal articles, 100 conference papers, and holds nine patents for electrical engineering application. His research interests include high voltage, high power and high efficiency conversion technology, renewable energy conversion technology, power system, and lighting technology.

Yi-Ping Hsieh was born in Tainan, Taiwan, in 1986. He received the B.S., M.S., and the Ph.D degrees in electrical engineering from National Cheng-Kung University, Taiwan, in 2008, 2010, and 2013, respectively.

He was a Postdoctoral Fellow in 2013. Currently, he is an R&D engineer with the UPS BU, Delta Electronics Corporation, Tainan, Taiwan. His research interests include circuit topologies, power factor correction, power converter, renewable energy conversion, and lighting.